공학석사학위논문

Highly Sensitive Ultrathin Image Sensor Inspired by Tapetum Lucidum

휘판 구조에서 착안한

고감도 초박막 이미지 센서

2020년 8월

서울대학교 대학원

협동과정 바이오엔지니어링

조효진

Highly Sensitive Ultrathin Image Sensor Inspired by Tapetum Lucidum

A THESIS SUBMITTED IN PARTIAL FULFILLMENT OF THE REQUESTMENTS FOR THE DEGREE OF MASTER IN ENGINEERING AT THE GRADUATE SCHOOL OF SEOUL NATIONAL UNIVERSITY

August 2020

By

Hyojin Cho

Supervisor

Dae-Hyeong Kim

Abstract

Highly Sensitive Ultrathin Image Sensor Inspired by Tapetum Lucidum

Hyojin Cho

Interdisciplinary Program for Bioengineering

The Graduate School

Seoul National University

High sensitivity imaging under the both bright and dim light condition is an important feature required in many emerging applications of the machine vision such as unmanned vehicles, aerial drones, etc. In nature, owing to the unique optics of tapetum lucidum, the eye of cats is well-known for maintaining excellent sensitivity regardless of varying light intensities. Here, we propose a bioinspired imaging device that enables the high sensitivity imaging under both dim and bright illumination. Inspired by the scotopic vision of the cat, the proposed

imaging device comprises of an ultrathin hemispherical photodetector array integrated with underlying artificial tapetum. The image sensor in hemispherical geometry, which is a common retinal structure for biological eyes, can achieve minimum optical aberration by using a simple configuration of lens. Submicron thickness of silicon enables the hemispherical structure without performance degradation. Patterned inverse opal structure is used as the artificial tapetum, which increases the light absorption by reflecting the transmitted light back to the photodiode. Theoretical optical analysis and experimental validations proved this novel feature of the proposed imaging device.

Keywords: Flexible electronics, Bio-inspired image sensor, Curved image sensor, Patterned photonic crystal, Tapetum lucidum.

Student number: 2018-21164

Contents

List of Schemes

List of Figures

1. Introduction

As technologies such as autonomous vehicles, aerial drones, and wearables, which are in the spotlight recently, require visual information to communicate with the external system, there is a growing need to develop imaging system equipped with various features such as wide field-of-view (FoV), miniaturization, and low light imaging[1,2]. While conventional approaches focused on changing existing optical and electrical components in typical camera structure for that, there have been obstacles like limited field of view, optical aberration due to its flat geometry, and complex lens optics[3] (**Scheme 1**). Instead, there have been the other approaches, that are inspired by the eyes of animals changing overall structure of the imaging device[4–8] (**Figure 1**). These biomimicry imaging devices commonly share the hemispherical geometrics for wide FoV and aberration-free imaging with simple lens optics, thus requiring ultrathin optoelectronics to endure the shape deformation[9–12]. However, lowering the thickness of active layer results in weak light absorbance, which degrades photosensitivity and absorption uniformity. Therefore, in the demand of absorbance enhancement for low light imaging, light sensitivity enhancement mechanism from feline eye inspired the proposed imaging device.

The cats have the crepuscular behavior, so their most active time is dawn and

dusk[13]. To adapt under such a dim light condition, they evolved to have a sensitive scotopic vision with a fully dilated pupil and a multi-layered tissue, tapetum lucidum (**Figure 2**)[14–17]. Although the dilated pupil sacrifices the depth-of-field (DoF) due to its fully-rounded aperture, it allows more light to the retina[18–21]. Moreover, tapetum lucidum enhances the retinal sensitivity by reflecting the incident light back to the retina, which makes the eye of the cat shine in the dark (**Figure 2**, inset)[16]. Tapetum lucidum is placed between the retina and the choroid (**Scheme 2**). Periodically repetitive rectangular cells containing bundles of parallel crystal rods comprises the tapetum lucidum. Each rectangular cell, bundle of rods (n = 1.83) and cell matrix (n = 1.33), can be simplified as a multi-layered reflector with alternating high and low refractive index (**Scheme 2, inset**). In this structure, the Bragg's law can be applied[22]. The incident light with a specific wavelength, which is determined by the thickness and refractive index of each layer, is reflected at every interface and contributes to the constructive interference, which can be accumulated by increasing the number of repeated layers[23–27].

Many emerging technologies based on the artificial vision require to obtain high-quality visual information under varying external light intensities. And such unique features of the feline eye, which maintains the excellent visual sensitivity under both bright and dim environments, have inspired a novel imaging device. Here, a biomimetic image sensor with enhanced light sensitivity is proposed. The

proposed imaging device consists of an ultrathin hemispherical silicon photodetector array and a patterned inverse opal (IO) reflector. Each component resembles the feline retina and tapetum lucidum respectively[28–31]. Due to the submicron thickness of the photodetector, it endures mechanical deformation into hemispherical shape without damaging the device performance[32]. Also, the patterned IO reflector enhances the light sensitivity under a dim environment[32–35]. The feline-eye-inspired artificial vision provides the new concept for the next generation image sensor.

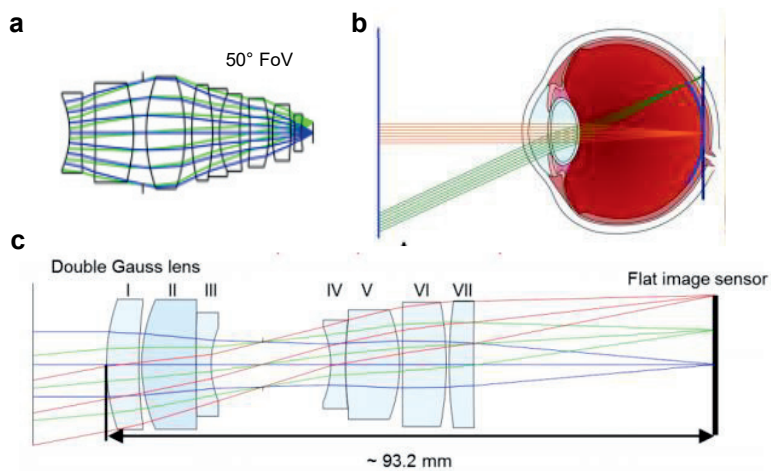

Scheme 1. (a) Schematic illustration showing limited field of view of conventional flat image sensor[11]. (b) Schematic description of optical aberration that occurs at flat image sensor compared to curved retina[11]. (c) Schematic diagram of complex lens module of conventional image sensor[7].

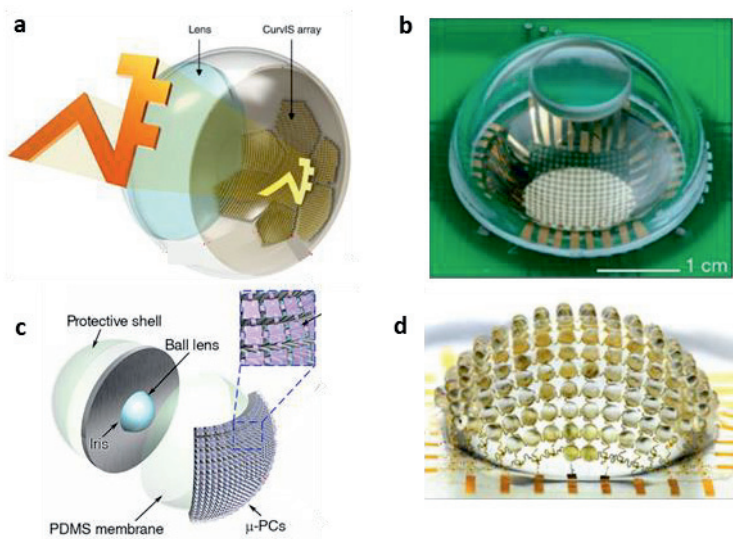

Figure 1. Bio-inspired image sensor (a) Schematic illustration showing the system of human-eye-inspired curved image sensor[6]. (b) Photograph of the hemispherical electronic eye camera[12]. (c) Schematic diagram of artificial eye inspired by the scotopic vision of elephantnose fish[8]. (d) Photograph of the digital camera inspired by the arthropod eye[7].

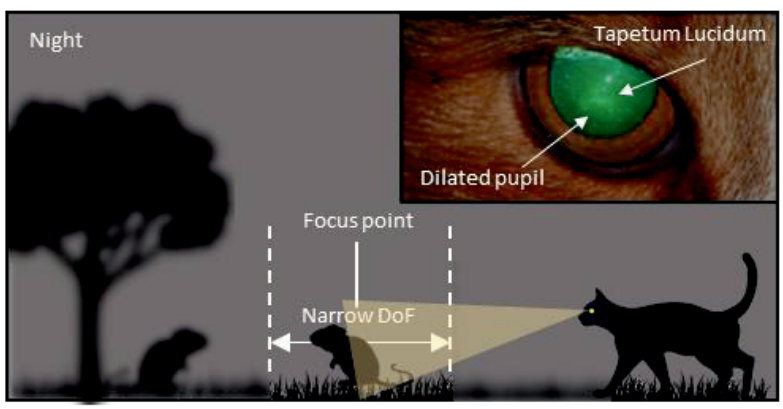

Figure 2. Schematic illustration showing crepuscular behavior of cat under dark illumination. The distinct region shows narrow depth of field due to the dilation of pupil. The inset shows dilated circular pupil and the light reflection from the tapetum lucidum.

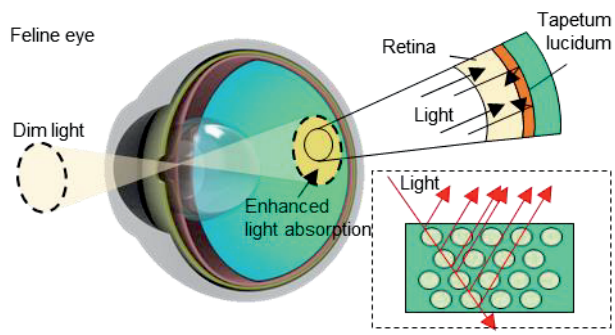

Scheme 2. Schematic diagram of cat's highly sensitive eye structure. The magnified view of retina shows the position of tapetum lucidum. The inset shows the light absorption enhancement mechanism inside the tapetum lucidum.

2. Design of artificial tapetum for ultrathin photodiode image sensor array

2.1 Optical characterization of ultrathin photodiode with artificial tapetum

A single pixel of the photodetector array consists of ultrathin photodiode and artificial tapetum (**Scheme 3**). Because of the submicron thick silicon layer, most of the irradiated light is transmitted at the silicon and polyimide layer without absorption. IO reflector is used for the artificial tapetum, of which photonic bandgap is determined by refractive index variation of periodically repetitive structure. Incident light having larger energy than the photonic bandgap energy of the artificial tapetum is reflected back to the silicon layer. Due to the optical path elongation inside the silicon layer, the light absorption in silicon layer is increased. In **Figure 3**, the light absorption inside the silicon layer (300 nm) decreases with wavelength, but the absorption loss in silicon layer is compensated by the artificial tapetum.

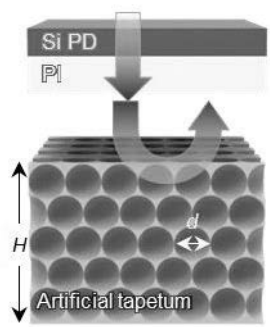

Scheme 3. Schematic description of optical path at ultrathin photodiode with artificial tapetum.

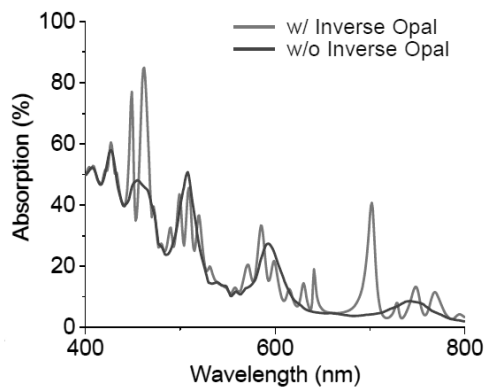

Figure 3. Absorbance spectrum of 300nm silicon and calculated enhanced absorption with the artificial tapetum.

2.1 Optimization for specification of artificial tapetum

For the optimization of absorption enhancement in silicon photodiode, optical simulations are conducted by varying void diameters of 400 nm, 550 nm, and 700 nm. Considering absorption coefficient of the Si nanomembrane, simulation results show the absorbance spectrum in silicon layer corresponding to the reflectance in artificial tapetum (**Figure 4**). The reflectance peak of each diameter is shifted to longer wavelength when the void diameter increases. Void diameter of 550 nm has the highest intensity at the peak compared to other absorption spectra. A void diameter larger than 400nm shows the non-zeroth order peak formation, so light absorption is enhanced compared to the diameter smaller than 400 nm. **Figure 5** shows the calculated averaged absorption in Si layer with varying void diameter. The void diameter of 550 nm shows the highest absorption enhancement in Si layer according to the simulation result.

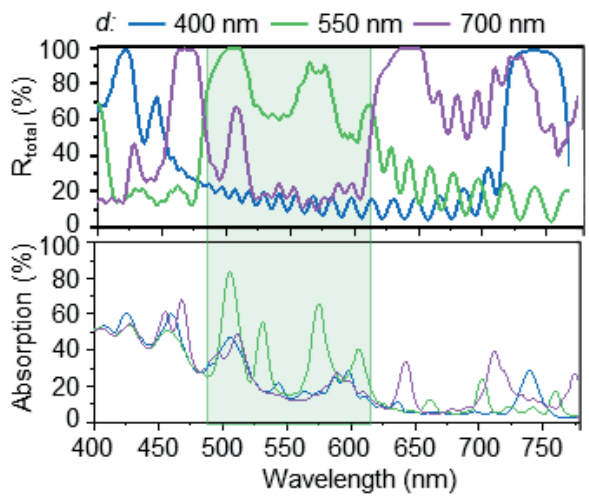

Figure 4. Simulation of reflection and absorption spectrum by varying diameters of 400nm, 550nm, and 700nm.

Figure 5. Simulation of absorption enhancement with varying particle

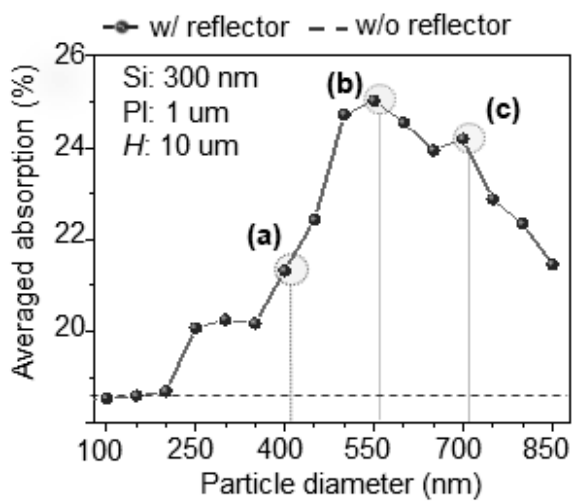

diameter size and same height of 10 µm.

3. Integration of artificial tapetum with ultrathin photodiode array

Inspired by the structure of the feline eye, the photodetector array with the artificial tapetum are fabricated on a hemispherical dome to reduce optical aberration and improve visual sensitivity. Since the thickness of the proposed imaging device increases due to the artificial tapetum, the IO matrix material needs to have low Young's modulus compared to that of Si for the mechanical deformability. Moreover, scattering of incident light into adjacent pixel should be prevented because it degrades the accuracy of imaging result. Thus, we fabricated patterned inverse opal reflector by using a low-modulus polymer (11 MPa) via lift-off process and tear-assisted patterning (TAP) process.

3.1 Fabrication of patterned opal by lift-off process

Scheme 4 illustrates the lift-off process which converts colloidal particles into patterned opal. i) thin film of SiO_2 is sputtered and spin-coated Teflon layer is stacked on the encapsulated photodetector array for an adequate adhesion at the lift-off process. Next, 1 um thick parylene-C and chromium (Cr) layers are stacked in order and patterned as a sacrificial layer. ii) the device is suspended in 550nm size colloidal silica and the dried at convection oven (65 ℃). SiO_2 opal film is self-assembled in a face-centered cubic (fcc) structure above the sacrificial layer and device. iii) parylene-Cr film is lifted off from the device and the patterned silica opal structure is left on each pixel. **Figure 6** shows the images of patterned opal after the lift-off process. Pattern size was varied from 10 μm to 1 mm. Regardless of the pattern size, uniform patterning of colloidal crystals was confirmed with the results.

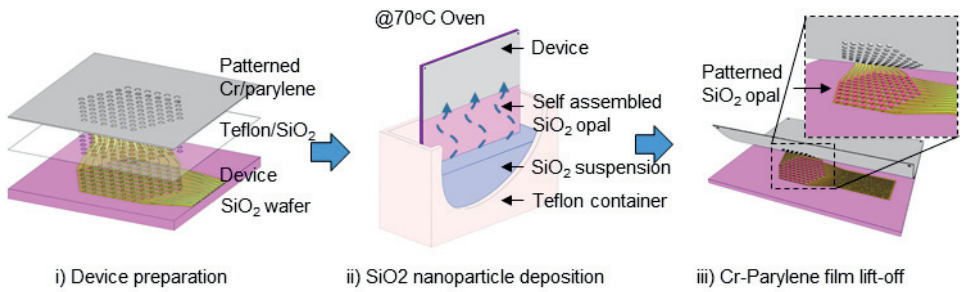

Scheme 4. Schematic illustration of lift-off process for patterning opal.

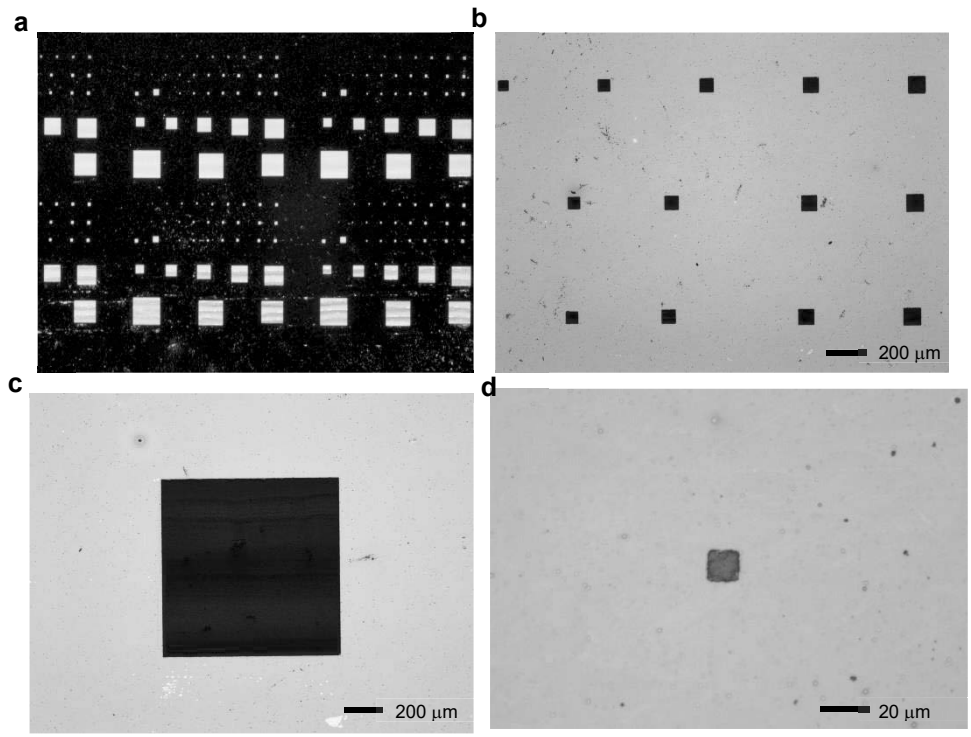

Figure 6. (a) Photograph showing the array of patterned opal with various size. (b) Optical microscope (OM) images showing patterned opal array consisted of size under 100 μm. (c), (d) OM image showing 1 mm, 10 μm size patterned opal through the lift-off process.

3.2 Fabrication of patterned inverse opal by TAP process

Scheme 5 shows the procedure of TAP process. First, UV curable polymer (NOA 73) is infiltrated into the space between the particles by capillary action, while it maintains fcc structure. Second, NOA infiltrated opal film is partially cured with UV light. Then, shear stress is silica-NOA composite and tear propagates along the interface of bulk NOA and the composite. As the surface except the area of composite was covered with Teflon during the lift-off process which was explained at previous section, the bulk NOA 73 is easily removed from the substrate. The patterned composite remains above each pixel, and is fully cured with UV. Lastly, the device is suspended in diluted HF solution to remove silica nanoparticles and NOA 73 inverse opal structure is left behind. **Figure 7** shows the images of patterned inverse opal after the TAP process. Pattern size was varied from 10 μm to 1 mm. Area of pattern was preserved without damage and uniform patterning of inverse opal was conducted regardless of the size variation.

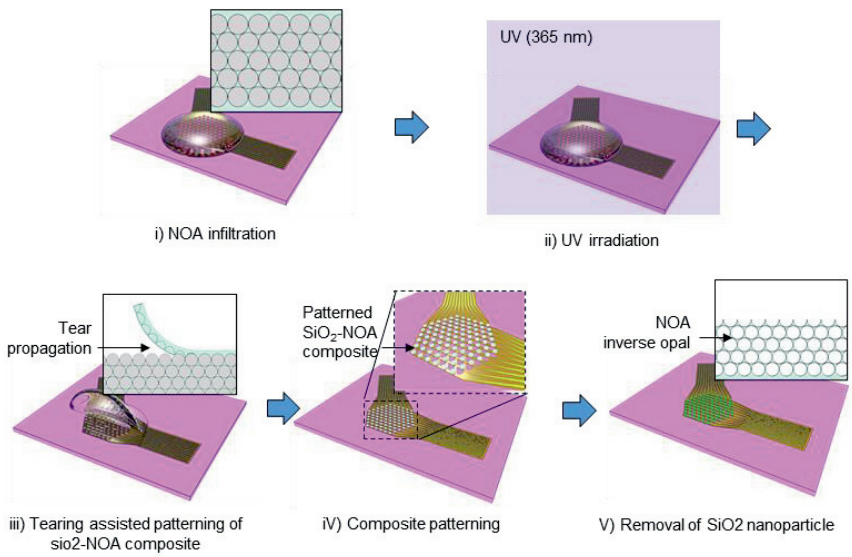

Scheme 5. Schematic description for TAP process for patterned inverse opal.

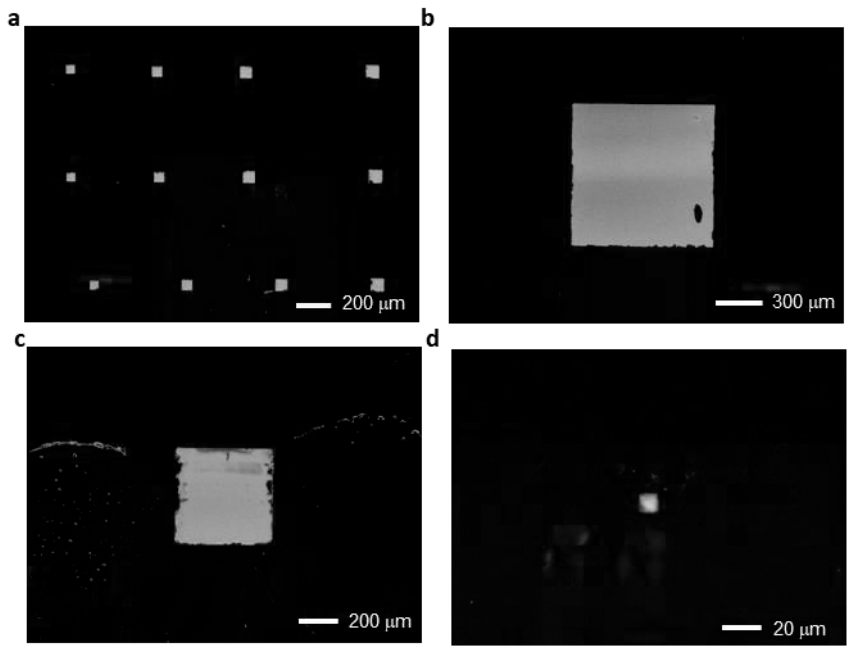

Figure 7. (a) Optical microscope (OM) images showing patterned inverse opal array consisted of size under 100 μm. (b), (c), (d) OM image showing 1 mm, 500 μm and 10 μm size patterned inverse opal through the TAP process.

3.2 Characterization of the proposed patterning process

Reflectance spectra are measured to analyze the optical characteristics of the artificial tapetum, which is the patterned inverse opal (**Figure 8**). Since the silica nanoparticles were stacked in fcc structure, reflectance spectrum of the opal shows the peak around 650 nm wavelength and uniform red color appears in the optical microscope (OM) image (**Figure 9a**). However, for the NOA-silica composite, refractive index contrast between matrix (n = 1.56) and particle (n = 1.5) decreases due to infiltrated NOA inside the interstices of opal structure. As a result, the peak of the reflectance spectrum is red-shifted to wavelength of 723 nm and the color and intensity of the composite are weak compared to the opal (**Figure 9b**). For the inverse opal structure, air cavity (n = 1) replaces the particle (n = 1.5), which results in increase in refractive index contrast between the cavity and matrix. Thus, reflectance peak of the inverse opal is blue-shifted to wavelength of 520 nm which forms yellow color in OM image (**Figure 9c**).

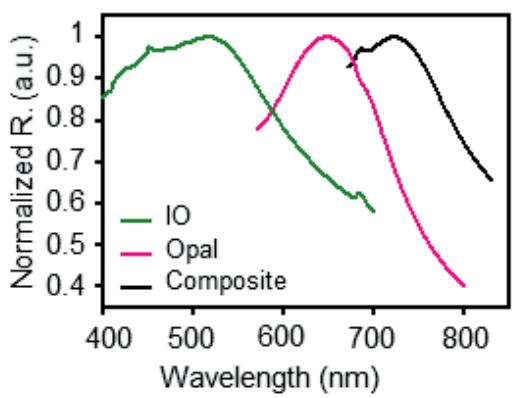

Figure 8. The reflectance spectra of opal, composite, and inverse opal films.

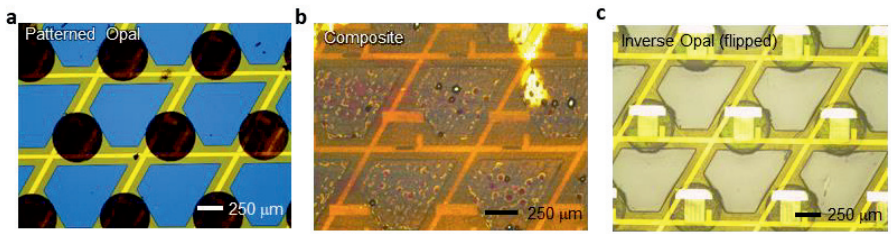

Figure 9. Optical microscope (OM) images of (a) the patterned opal, (b) composite and (c) inverse opal on the ultrathin photodiode array.

4. Ultrathin hemispherical image sensor with artificial tapetum

4.1 Image sensor array with patterned artificial tapetum on curved surface

Figure 10a shows the ultrathin photodetector array integrated with the patterned inverse opal on a hemispherical surface. As the tapetum lucidum of feline eye reflects the light and makes eye shine in dark environment, reflection from the artificial tapetum under dim light can be observed from the inset (**Figure 10b**). The scanning electron microscope (SEM) image shows the top and sectioned view of the device with polymeric artificial tapetum **(Figure 11**, **12**). Each pixel resembles the structural and functional characteristics of tapetum lucidum in feline eye. Inside the polymeric matrix, the air holes are formed in fcc arrangement after the lift-off and TAP process.

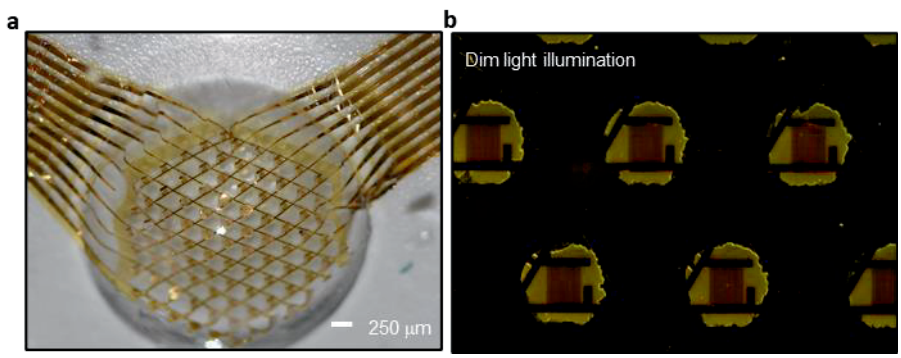

Figure 10. (a) The photograph of ultrathin hemispherical photodiode array with artificial tapetum. (b) Optical microscope (OM) image of the array under low illumination.

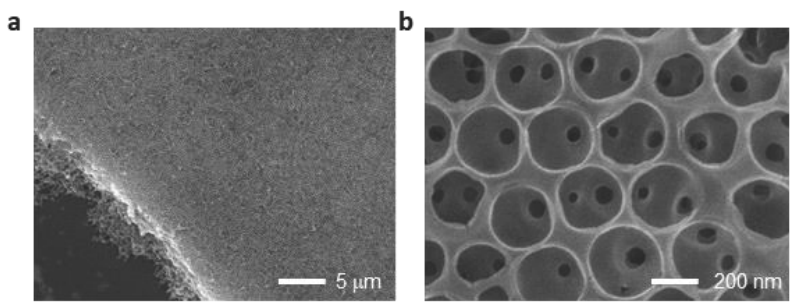

Figure 11. (a) Scanning electron microscopy (SEM) images of the artificial tapetum on photodiode. (b) Magnified view of the artificial tapetum on photodiode.

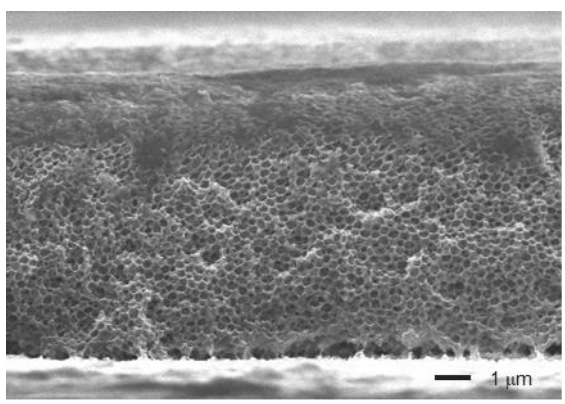

Figure 12. Cross-sectional scanning electron microscopy (SEM) images of the artificial tapetum on photodiode.

4.2 Electrical characteristics of an ultrathin image sensor with artificial tapetum

The photo-absorption of 300nm thick bare Si decreases as the wavelength increases, so the wavelength longer than 500nm penetrates through the silicon without absorption (**Figure 13**). For the proposed imaging device, ultrathin Si photodiodes (t = 300 nm) in lateral configuration are used for improving mechanical deformability in curved shape. To compensate the absorption loss in long wavelength in ultrathin silicon, polymeric IO are used. The photodiode with artificial tapetum shows enhanced light sensitivity compared to the photodiode without IO because it has the elongated optical path (**Figure 14**). Moreover, photodiode with the artificial tapetum shows improved photo-sensitivity (2.15 A/W) compared to the photodiode without the artificial tapetum (1.52 A/W) (**Figure 15**). The temporal photocurrent response under dim environment, same as the light intensity under moonlight (< 1 lux), was measured at the bias of 1V. The photodiode with the artificial tapetum showed high contrast on rise/fall process (**Figure 16**).

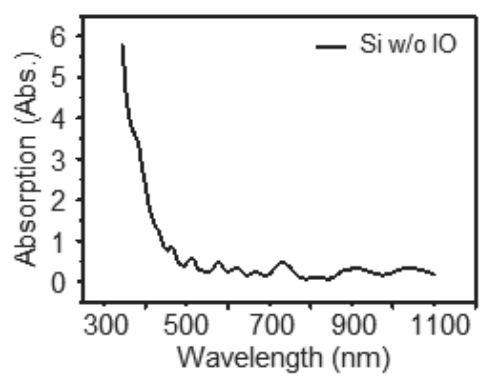

Figure 13. Absorption spectrum of bare Si.

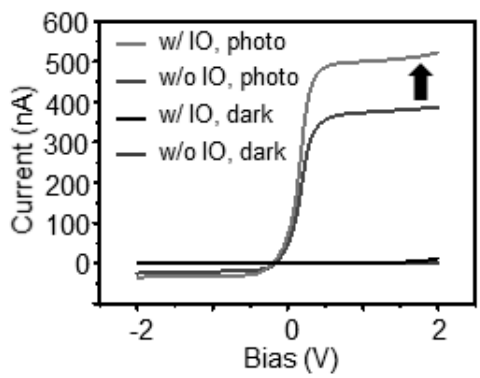

Figure 14. *I-V* curve of a single photodiode with inverse opal and a single photodiode without inverse opal under dark condition and bright condition.

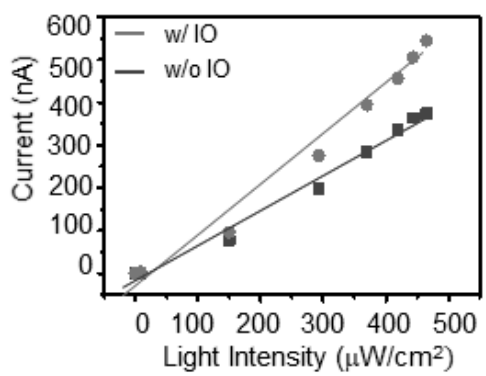

Figure 15. Plot of current versus irradiance showing linearity with different light intensities.

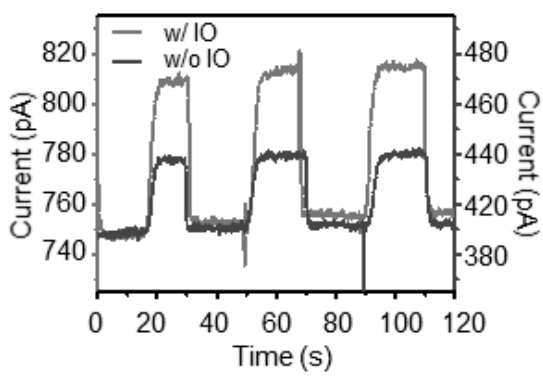

Figure 16. Temporal response of an ultrathin Si photodiode with inverse opal and without inverse opal.

4.3 Imaging characterization of feline-eye-inspired artificial vision

The ultrathin hemispherical photodiode array integrated with artificial tapetum is transferred to a hemispherical surface. **Scheme 6** shows the experimental setup for imaging demonstration. In the setup, shadow mask with pattern is mounted on a light source to filter the light selectively (**Figure 17**). The aperture controls the amount of light irradiated on the image sensor. The fully integrated photodiode array is connected to the external measurement setup by anisotropic conductive film (ACF).

Figure 18 shows the successful image acquisition of pattern 'S' and inverted 'Σ' using a single plano-convex lens. The original pattern is shown in the left side**.** The feline-eye-inspired artificial vision achieved sensitive capture of various images with enhanced sensitivity.

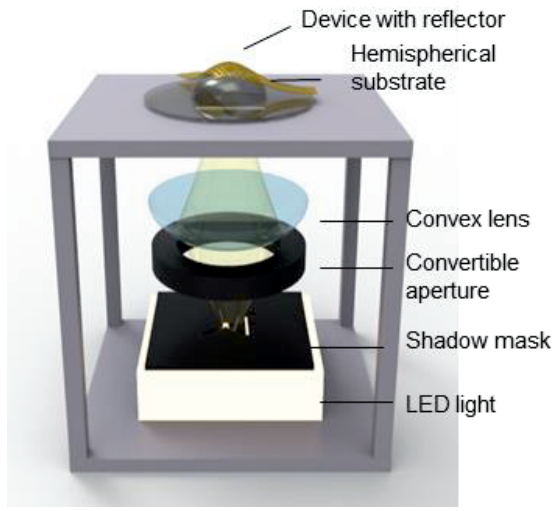

Scheme 6. Schematic illustration showing experimental setup for imaging demonstration.

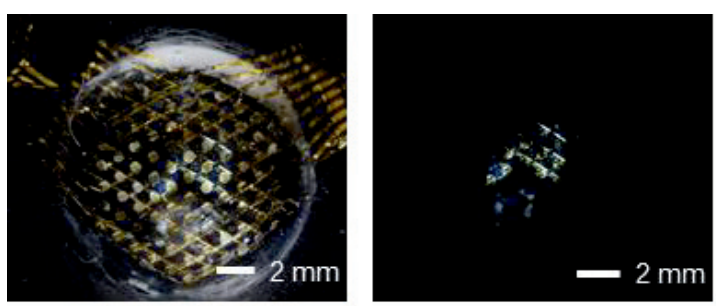

Figure 17. Optical camera image of patterned light irradiated on the image sensor array under different ambient illumination.

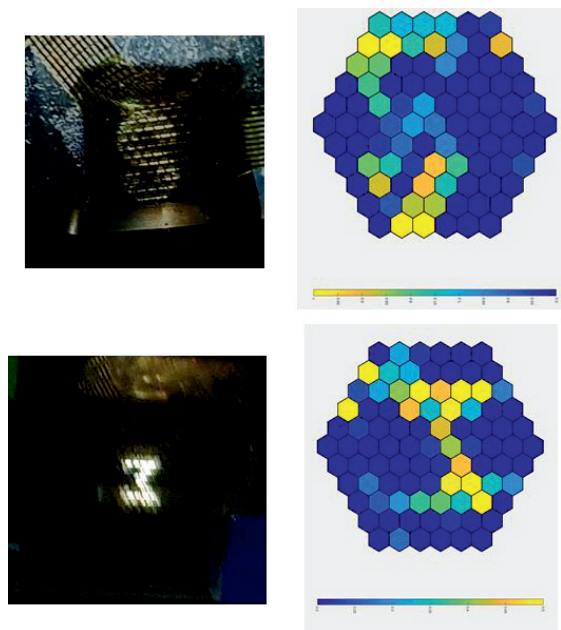

Figure 18. S, inverted Σ shaped image captured by ultrathin hemispherical photodiode array with artificial tapetum.

5. Experimental section

5.1 Fabrication of ultrathin photodiode array

Silicon-on-insulator wafer (340-nm-thick silicon layer on a silicon dioxide insulator layer, Soitec) was doped with spin-on-dopant. The individual photodiode had n-p-n configuration with serial connection. After the doping process, the silicon-on-insulator wafer was immersed in concentrated hydrofluoric acid to remove the buried SiO_2 layer. The doped regions were transferred onto 3.5 cm x 4 cm size SiO_2 wafer coated with polyimide (PI). The doped regions were isolated into an individual cell by reactive-ion etching with photolithography. PI was spin-coated on the top of the Si diode layer as the first dielectric layer. Through photolithography and dry etching process, VIA pattern was formed and Cr/Au layers (10/100 nm) were deposited on it by thermal evaporation. The Cr/Au layers were wet etched and formed the first electrode. Additional PI was spin-coated and cured as a dielectric layer. 2^{nd} VIA patterning and the deposition of Cr/Au for 2^{nd} metallization was conducted by using the same process as 1^{st} metallization. The device was encapsulated with 1 μm thickness PI and then the entire PI was etched into the final device pattern with reactive-ion etching process.

5.2 Patterned opal deposition on image sensor array

SiO_2 was deposited by RF sputtering under 20 sccm, 9m Torr Ar atmosphere at 50W RF power as an interfacial layer. Teflon amorphous fluoropolymers (Teflon AF) was spin-coated and cured at 180 ℃ for 5 minutes and 330 ℃ for 15 minutes subsequently for managing the adhesion between layers. Then, 1μm thickness of parylene-C film was deposited on the device and Cr (40 nm) was deposited by thermal evaporation. Cr film was etched into negative pattern of artificial tapetum through photolithography and wet etching process. The exposed parylene-C film was etched by reactive-ion etching and the SiO_2 interfacial layer will protect the device layer from over-etch. The surface of the patterned Cr and exposed device was treated by reactive-ion etching under 100 sccm, 0.1 Torr O atmosphere at 30W for 30s. The device was vertically dipped in a Teflon dish filled with the 0.2 wt% of silica nanoparticles in aqueous dispersion and the solvent was evaporated for 12 hours in the 70 ℃ convection oven. The opal structure was formed in a fcc structure. Cr-parylene film was easily lifted-off from the substrate without tear due to the Teflon treated surface and the opal was patterned into the array of circular reflectors.

5.3 Fabrication of patterned inverse opal on image sensor array

Patterned opal on image sensor array was infiltrated with Norland Optical Adhesive 73 (NOA 73) and placed in vacuum chamber for 5m. The infiltrated opal structure was irradiated with ultraviolet (UV) light and the cured bulk NOA 73 was removed by tweezer. NOA 73-silica composite remained on the substrate and was fully cured with additional UV irradiation. The composite was immersed in diluted HF solution for 5 minutes to remove the silica nanoparticles in the NOA 73 matrix.

5.4 *I-V* characterization of a single photodiode with artificial tapetum

The I-V characterization was performed by applying DC voltage from -2V to 2V and the corresponding current was measured by semiconductor device analyzer, B1500A (Agilent Technologies, USA). Probe station, MST-5500B (MS Tech, Korea) connected the image sensor array and the semiconductor device analyzer. To change the ambient illumination, FOK-100W (Fiber Optic Korea, Korea) was used. For the bright condition, white light of $465\mu\Omega/cm^2$ was irradiated on the device.

5.5 Reflectance spectrum characterization of photonic

crystals

A bare glass substrate was treated by Reactive Ion Etching (RIE) for 30s with 30W, 0.1 torr. Next, the glass substrate was dipped in a Teflon dish filled with 0.2wt% of silica nanoparticles in aqueous dispersion. Opal film was formed at the surface of the substrate. Then, the opal film was infiltrated by Norland Optical Adhesive 73 (NOA 73), which turns into silica-NOA 73 composite. The composite film was immersed in a diluted HF solution (5%) for 5 minutes and inverse opal structure was formed. The reflectance spectra of each photonic crystals were characterized by UV-VIS spectroscopy, V-770 (JASCO, Japan).

5.6 Absorption spectrum characterization of silicon with NOA 73 inverse opal

Silicon-on-insulator (SOI) wafer (340-nm-thick silicon layer on a silicon dioxide insulator layer, Soitec) was prepared in the size of 3 cm x 3cm, and the buried oxide layer was wet-etched by hydrofluoric acid (49.0%) for 20 minutes. Polyimide precursor solution was spin-coated on a bare glass substrate and cured shortly. The silicon layer of SOI wafer was transferred onto the PI-glass substrate and fully cured. Additional PI was spin-coated for encapsulation of silicon layer and cured on hotplate. The surface of fully cured PI was treated with reactive-ion etching for making hydrophilic surface for opal deposition. Opal layer was

deposited on the surface of PI through evaporation of 0.2 wt% silica nanoparticle in aqueous dispersion. Infiltration of NOA 73 and removal of silica nanoparticles in diluted hydrofluoric acid were performed. PI-Si-PI tri-layer device with inverse opal structure was used as an experimental device and PI-Si-PI tri layer device without inverse opal structure was used as a control device for absorption characterization. Absorption spectrum characterization was performed with UV-VIS spectroscopy, V-770 (JASCO, Japan).

6. Conclusion

In this paper, the unique feature of feline eye, which is the high sensitivity vision under varying illumination condition, inspires the image sensor array with artificial tapetum. Ultrathin photodiode array achieves enhanced light sensitivity and outstanding mechanical property by integration with artificial tapetum, composed of patterned inverse opal. Patterned inverse opal is polymerized NOA 73 matrix with air cavity, which has relatively low modulus and is designed to compensate the photo-absorption weakness of thin silicon at longer wavelength. We validated the proposed features of the whole integrated device through theoretical analyses and imaging demonstrations. Feline-eye-inspired artificial vision is expected to contribute to the development of imaging with enhanced sensitivity and unconventional imaging device.

7. References

1. Floreano, D.; Wood, R. J. Science, Technology and the Future of Small Autonomous Drones. *Nature* **2015**, *521* (7553), 460–466.
2. Jafferis, N. T.; Helbling, E. F.; Karpelson, M.; Wood, R. J. Untethered Flight of an Insect-Sized Flapping-Wing Microscale Aerial Vehicle. *Nature* **2019**, *570* (7762), 491–495.
3. Chung, T.; Lee, Y.; Yang, S. P.; Kim, K.; Kang, B. H.; Jeong, K. H. Mining the Smartness of Insect Ultrastructures for Advanced Imaging and Illumination. *Adv. Funct. Mater.* **2018**, *28* (24), 1–14.
4. Lee, L. P.; Szema, R. Inspirations from Biological Optics for Advanced Photonic Systems. *Science (80-.).* **2005**, *310* (5751), 1148–1150.
5. Keum, D.; Jang, K. W.; Jeon, D. S.; Hwang, C. S. H.; Buschbeck, E. K.; Kim, M. H.; Jeong, K. H. Xenos Peckii Vision Inspires an Ultrathin Digital Camera. *Light Sci. Appl.* **2018**, *7* (1).
6. Choi, C.; Choi, M. K.; Liu, S.; Kim, M. S.; Park, O. K.; Im, C.; Kim, J.; Qin, X.; Lee, G. J.; Cho, K. W.; Kim, M.; Joh, E.; Lee, J.; Son, D.; Kwon, S. H.; Jeon, N. L.; Song, Y. M.; Lu, N.; Kim, D. H. Human Eye-Inspired Soft Optoelectronic Device Using High-Density MoS2-Graphene Curved Image Sensor Array. *Nat. Commun.* **2017**, *8* (1).
7. Song, Y. M.; Xie, Y.; Malyarchuk, V.; Xiao, J.; Jung, I.; Choi, K. J.; Liu, Z.; Park, H.; Lu, C.; Kim, R. H.; Li, R.; Crozier, K. B.; Huang, Y.;

Rogers, J. A. Digital Cameras with Designs Inspired by the Arthropod Eye. *Nature* **2013**, *497* (7447), 95–99.

8. Liu, H.; Huang, Y.; Jiang, H. Artificial Eye for Scotopic Vision with Bioinspired All-Optical Photosensitivity Enhancer. *Proc. Natl. Acad. Sci. U. S. A.* **2016**, *113* (15), 3982–3985.
9. Wu, T.; Hamann, S. S.; Ceballos, A. C.; Chang, C. E.; Solgaard, O.; Howe, R. T. Design and Fabrication of Silicon-Tessellated Structures for Monocentric Imagers. *Microsystems Nanoeng.* **2016**, *2*.
10. Zhang, K.; Jung, Y. H.; Mikael, S.; Seo, J. H.; Kim, M.; Mi, H.; Zhou, H.; Xia, Z.; Zhou, W.; Gong, S.; Ma, Z. Origami Silicon Optoelectronics for Hemispherical Electronic Eye Systems. *Nat. Commun.* **2017**, *8* (1).
11. Guenter, B.; Joshi, N.; Stoakley, R.; Keefe, A.; Geary, K.; Freeman, R.; Hundley, J.; Patterson, P.; Hammon, D.; Herrera, G.; Sherman, E.; Nowak, A.; Schubert, R.; Brewer, P.; Yang, L.; Mott, R.; McKnight, G. Highly Curved Image Sensors: A Practical Approach for Improved Optical Performance. *Opt. Express* **2017**, *25* (12), 13010.
12. Ko, H. C.; Stoykovich, M. P.; Song, J.; Malyarchuk, V.; Choi, W. M.; Yu, C. J.; Geddes, J. B.; Xiao, J.; Wang, S.; Huang, Y.; Rogers, J. A. A Hemispherical Electronic Eye Camera Based on Compressible Silicon Optoelectronics. *Nature* **2008**, *454* (7205), 748–753.
13. Sakmann, B.; Creutzfeldt, O. D. Scotopic and Mesopic Light Adaptation

in the Cat's Retina. *Pflügers Arch. Eur. J. Physiol.* **1969**, *313* (2), 168–185.

14. Schwab, I. R.; Yuen, C. K.; Buyukmihci, N. C.; Blankenship, T. N.; Fitzgerald, P. G.; Eagle, R. C.; Sadun, A. A.; Ernest, T. J. Evolution of the Tapetum. *Trans. Am. Ophthalmol. Soc.* **2002**, *100*, 187–200.
15. Braekevelt, C. R. Fine Structure of the Tapetum Lucidum of the Paca Cuniculus Paca. *Acta Anat. (Basel).* **1993**, *146* (4), 244–250.
16. Ollivier, F. J.; Samuelson, D. A.; Brooks, D. E.; Lewis, P. A.; Kallberg, M. E.; Komáromy, A. M. Comparative Morphology of the Tapetum Lucidum (among Selected Species). *Vet. Ophthalmol.* **2004**, *7* (1), 11–22.
17. Pedler, C. The Fine Structure of the Tapetum Cellulosum. *Exp. Eye Res.* **1963**, *2* (2), 189–195.
18. González-Martín-Moro, J.; Gómez-Sanz, F.; Sales-Sanz, A.; Huguet-Baudin, E.; Murube-del-Castillo, J. Pupil Shape in the Animal Kingdom: From the Pseudopupil to the Vertical Pupil. *Arch. la Soc. Española Oftalmol. (English Ed.* **2014**, *89* (12), 484–494.
19. Banks, M. S.; Sprague, W. W.; Schmoll, J.; Parnell, J. A. Q.; Love, G. D. Why Do Animal Eyes Have Pupils of Different Shapes? *Sci. Adv.* **2015**, *1* (7), 1–10.
20. Hammond, P.; Mouat, G. S. V. The Relationship between Feline Pupil

Size and Luminance. *Exp. Brain Res.* **1985**, *59* (3), 485–490.

21. Douglas, R. H. The Pupillary Light Responses of Animals; a Review of Their Distribution, Dynamics, Mechanisms and Functions. *Prog. Retin. Eye Res.* **2018**, *66* (May), 17–48.

22. Lee, S. Y.; Kim, S. H.; Hwang, H.; Sim, J. Y.; Yang, S. M. Controlled Pixelation of Inverse Opaline Structures towards Reflection-Mode Displays. *Adv. Mater.* **2014**, *26* (15), 2391–2397.

23. Min, K.; Kim, S.; Kim, S. Deformable and Conformal Silk Hydrogel Inverse Opal. *Proc. Natl. Acad. Sci. U. S. A.* **2017**, *114* (24), 6185–6190.

24. Lee, J. W.; Moon, J. H. Monolithic Multiscale Bilayer Inverse Opal Electrodes for Dye-Sensitized Solar Cell Applications. *Nanoscale* **2015**, *7* (12), 5164–5168.

25. Varghese, L. T.; Xuan, Y.; Niu, B.; Fan, L.; Bermel, P.; Qi, M. Enhanced Photon Management of Thin-Film Silicon Solar Cells Using Inverse Opal Photonic Crystals with 3D Photonic Bandgaps. *Adv. Opt. Mater.* **2013**, *1* (10), 692–698.

26. Chiu, W.; Wu, Y.; Chan, Y.; Hou, C. H.; Chien, H. T.; Chen, C. C. Photonic Crystal Filter Integrated With Photodiodes. *15th Eur. Conf. Integr. Opt. ECIO 2010* **2010**, *2*, 52–53.

27. Hwang, D. K.; Noh, H.; Cao, H.; Chang, R. P. H. Photonic Bandgap Engineering with Inverse Opal Multistacks of Different Refractive Index

Contrasts. *Appl. Phys. Lett.* **2009**, *95* (9), 1–4.

28. Tuyen, L. D.; Wu, C. Y.; Anh, T. K.; Minh, L. Q.; Kan, H. C.; Hsu, C. C. Fabrication and Optical Characterisation of SiO 2 Opal and SU-8 Inverse Opal Photonic Crystals. *J. Exp. Nanosci.* **2012**, *7* (2), 198–204.
29. Xie, K.; Guo, M.; Huang, H. Photonic Crystals for Sensitized Solar Cells: Fabrication, Properties, and Applications. *J. Mater. Chem. C* **2015**, *3* (41), 10665–10686.
30. Kuai, S. L.; Hu, X. F.; Haché, A.; Truong, V. Van. High-Quality Colloidal Photonic Crystals Obtained by Optimizing Growth Parameters in a Vertical Deposition Technique. *J. Cryst. Growth* **2004**, *267* (1–2), 317–324.
31. Hatton, B.; Mishchenko, L.; Davis, S.; Sandhage, K. H.; Aizenberg, J. Assembly of Large-Area, Highly Ordered, Crack-Free Inverse Opal Films. *Proc. Natl. Acad. Sci. U. S. A.* **2010**, *107* (23), 10354–10359.
32. Gao, Y.; Cansizoglu, H.; Polat, K. G.; Ghandiparsi, S.; Kaya, A.; Mamtaz, H. H.; Mayet, A. S.; Wang, Y.; Zhang, X.; Yamada, T.; Devine, E. P.; Elrefaie, A. F.; Wang, S. Y.; Islam, M. S. Photon-Trapping Microstructures Enable High-Speed High-Efficiency Silicon Photodiodes. *Nat. Photonics* **2017**, *11* (5), 301–308.
33. Armstrong, E.; O'Dwyer, C. Artificial Opal Photonic Crystals and Inverse Opal Structures-Fundamentals and Applications from Optics to

Energy Storage. *J. Mater. Chem. C* **2015**, *3* (24), 6109–6143.

34. Üpping, J.; Bielawny, A.; Wehrspohn, R. B.; Beckers, T.; Carius, R.; Rau, U.; Fahr, S.; Rockstuhl, C.; Lederer, F.; Kroll, M.; Pertsch, T.; Steidl, L.; Zentel, R. Three-Dimensional Photonic Crystal Intermediate Reflectors for Enhanced Light-Trapping in Tandem Solar Cells. *Adv. Mater.* **2011**, *23* (34), 3896–3900.

35. Zhang, J.; Sun, Z.; Yang, B. Self-Assembly of Photonic Crystals from Polymer Colloids. *Curr. Opin. Colloid Interface Sci.* **2009**, *14* (2), 103–114.

요약 (국문초록)

휘판 구조에서 착안한 고감도 초박막 이미지 센서

서울대학교 공과대학원

바이오엔지니어링 협동과정

조효진

고양이의 눈은 휘판 구조와 외부의 조도에 따른 동공 반응으로 인해 어두운 환경에서부터 밝은 환경까지 높은 감도로 빛을 인지합니다. 본 논문에서는 생체 모방 방식을 통해 낮은 조도와 어두운 조도 모두에서 고감도의 이미징이 가능한 이미지 센서를 제시했습니다. 고양이의 암소시로부터 영감을 받아 제작한 이 이미지 센서는 초박막의 반구 형태의 광 다이오드 어레이가 인공 휘판 구조와 결합된 형태입니다. 반구 형태는 자연의 망막 구조와 같은 것으로 광 수차가 적은 이미징을 가능하게 합니다. 나노 두께의 실리콘은 이미지 센서의 성능을 저하시키지 않고

반구 형태로의 변형이 가능합니다. 인공 휘판 구조는 패터닝 된 인버스 오팔 구조로 이루어져 있으며, 이 구조는 광 다이오드에 흡수되지 않고 통과한 빛이 다시 광 다이오드로 반사되어 빛의 흡수율을 높이는 역할을 합니다. 이러한 특성은 이론적인 분석과 실험을 통해 증명되었습니다. 고양이의 눈에서 영감을 받은 인공 시각 시스템은 향후 기존의 이미징 시스템과는 차별점을 둔 새로운 이미지 센서의 개발에 기여할 것으로 예상됩니다.